ELSEVIER

Dynamics of Atmospheres and Oceans 27 (1997) 201–217

dynamics of atmospheres and oceans

Application of a modified Arakawa 'a' grid ocean model having reduced numerical dispersion to the Gulf of Mexico circulation

David E. Dietrich

Mississippi State University Center for Air Sea Technology, Albuquerque, NM 87112, USA

Received 28 January 1996; revised 16 September 1996; accepted 14 October 1996

Abstract

We describe a simple, flux conserving robust advection scheme that reduces numerical dispersion in application to passive scalar advection. Our hydrostatic semi-collocated (modified Arakawa 'a' grid) ocean model performance is enhanced by this modification in combination with a modified strategy for incompressibility. The modified advection scheme also reduces overshooting errors resulting from numerical dispersion in the evolution of a sloshing front using a non-hydrostatic model.

In Gulf of Mexico simulations, many of the realistic detailed features from our original model using $1/12^{\circ}$ (about 9 km) resolution occur using the modified numerics with 20-km resolution. These are not seen with the original numerics and 20-km resolution. These detailed features include: strong fronts and frontal eddies; many cyclonic eddies, which spin off major warm core Loop Current eddies; and sharp eastward deflection of the Loop Current directly into the Florida Strait after major warm core eddy shedding. © 1997 Elsevier Science B.V.

1. Introduction

The modified Arakawa 'a' grid DieCAST (Dietrich/Center for Air Sea Technology) (Dietrich et al., 1993, Dietrich and Ko, 1994) ocean model was derived from the modified Arakawa 'c' grid SOMS (Sandia ocean modeling system: Dietrich et al., 1987, Dietrich, 1992) ocean model. Both models are three-dimensional in a rotating frame, and use the hydrostatic, Boussinesq, and rigid-lid approximations. They use flux conserving centered approximations based on control volumes (Roache, 1976) and a weakly time-filtered leapfrog time integration scheme (Roache and Dietrich, 1988).

A significant feature is that both models use cubic interpolations to communicate data between collocated 'a' and staggered 'c' grid locations. Such mixed grid approaches

PII S0377-0265(97)00009-2

mitigate weak points of the respective grids (Coriolis terms on the 'c' grid; internal wave propagation terms on the 'a' grid). Higher order interpolations greatly improve grid convergence in prototype ocean problems (Dietrich et al., 1990, Dietrich, 1993).

Modified numerical schemes discussed in Section 2 further improve interpolations used by our models. The modified schemes are compared with our original ones in Section 3, with three applications: Section 3.1 applies to the classic cyclic passive scalar advection problem; Section 3.2 applies to a non-hydrostatic, Boussinesq, two-dimensional front; and Section 3.3 applies to a three-dimensional, hydrostatic Gulf of Mexico general circulation simulation.

2. Modified numerical schemes

2.1. Reduced dispersion advection scheme

Our first modification involves the interpolations used in advection. This scheme greatly reduces numerical dispersion, so we call it our reduced dispersion advection, or 'RDA', scheme. Our Arakawa 'a' grid model uses a 'c' grid non-divergent advection velocity. This desirable 'c' grid feature avoids null space problems in determining the pressure adjustment needed to get a non-divergent velocity. Our control volume 'a' grid advection scheme thus requires evaluation of the fluxed quantities at the staggered 'c' grid locations. The conventional advection scheme, used by our early ocean models, uses two-point averages, taking values from the scalar cell centers on each side of the cell faces, $1/2$ grid interval away:

$$f(i) = (f_{i-1/2} + f_{i+1/2})/2 \tag{1}$$

which is exact for linear variations.

Instead of two-point averages, our RDA scheme includes additional information from the next nearest points, $3/2$ grid intervals away:

$$f_i = \left[9(f_{i-1/2} + f_{i+1/2}) - f_{i-3/2} - f_{i+3/2}\right]/16 \tag{2}$$

which is exact for general cubic variations.

The resulting interpolated field is then multiplied by the non-divergent advection velocity to get the flux at the cell face. The fluxes are then substituted into the 'control volume' integrated conservation equations (Roache, 1976). While not leading to a formally higher order overall advection scheme, the new scheme is more accurate, conservative, and greatly reduces numerical dispersion.

2.2. Modified incompressibility algorithm

The second modification to our ocean model involves our numerical algorithm for construction of a non-divergent advection velocity, so we call it our modified incompressibility algorithm, or 'MIA' scheme. As with our original 'a' grid scheme (Dietrich et al., 1990), we determine the non-divergent advection velocity by: interpolating (using a cubic) the 'a' grid trial velocity (derived using a trial surface pressure, the hydrostatic

relation and the momentum equations) to the usual 'c' grid advection locations; then 'clearing out the divergence' of the resulting 'c' grid barotropic mode (vertically averaged) velocity by appropriate surface pressure adjustment and application. This incompressibility information must be communicated back to the 'a' grid locations.

Originally, we simply interpolated the 'c' grid advection velocity back to the 'a' grid locations, again using cubic fourth order as in the previous 'a' to 'c' grid interpolations. Although this combined forward/reverse interpolation is dispersive, the numerical dispersion effects are small when the time step is not small compared with the linear stability limit (Dietrich, 1993). Extremely small time step may result in artificial dispersion dominating other transients. Such artificial dispersion is greatly reduced by our new MIA scheme, allowing one to take advantage of the greatly reduced numerical dispersion of our RDA scheme described above, and thus achieve low overall numerical dispersion.

Our new MIA scheme uses a modified reverse interpolation approach. Instead of interpolating the 'c' grid velocity to the 'a' grid, we interpolate the *changes* of 'c' grid velocity that result from 'clearing out its divergence'. In other words, the interpolated changes are added to the original 'a' grid trial velocity referred to above. This procedure avoids any reverse interpolation effects if the changes are zero. (It seems possible to develop an expanded stencil 'a' grid pressure gradient operator corresponding to an expanded stencil Poisson operator which gives an 'a' grid velocity adjustment that when interpolated to the 'c' grid yields a non-divergent 'c' grid advection velocity. This procedure would avoid dispersive reverse interpolations, but would be more computationally intensive in the Poisson solver step.)

Combining this MIA scheme with our RDA (Section 2.1) scheme, the overall numerical dispersion is greatly reduced. The changes of velocity needed to maintain incompressibility are small compared with velocity differences at adjacent grid locations, because a good guess for the 'trial' top level pressure field is available each time step from previous results, thus producing a quasi-non-divergent velocity that requires only small adjustment to 'clear out its divergence'.

The MIA scheme is analogous to Scheme 2B (Dietrich et al., 1990) for the Coriolis terms in our original 'c' grid model, but is more effective because it greatly reduces numerical dispersion. We do not envision a correspondingly low dispersion 'c' grid scheme, because the interpolations needed for the Coriolis terms lead to significant dispersion even with Scheme 2B.

3. Comparison of modified and original schemes in three test problems

3.1. Classic cyclic passive scalar advection problem

Two-dimensional advection of a specified scalar feature in a cylindrical geometry with uniform angular velocity is widely used as a test case to show the properties of various advection schemes. Spectral methods are exact for such a linear advection problem and have good advection properties in general, while being expensive and limited in application.

The conventional centered control volume-based finite difference advection scheme used by our early ocean models, while having good total conservation properties, leads to substantial unphysical dispersion resulting from truncation errors. Nevertheless, realistic fronts and frontal eddies occur even in our original ocean models, because of their robustness with low explicit diffusion. The low explicit diffusion (large cell-Reynolds number) is robust, because the advection velocity tends to be nearly parallel to the iso-surfaces of the various fields, thus reducing the effective cell-Reynolds number compared with the usual scaling.

Here, we show that our modified advection scheme greatly reduces this numerical dispersion.

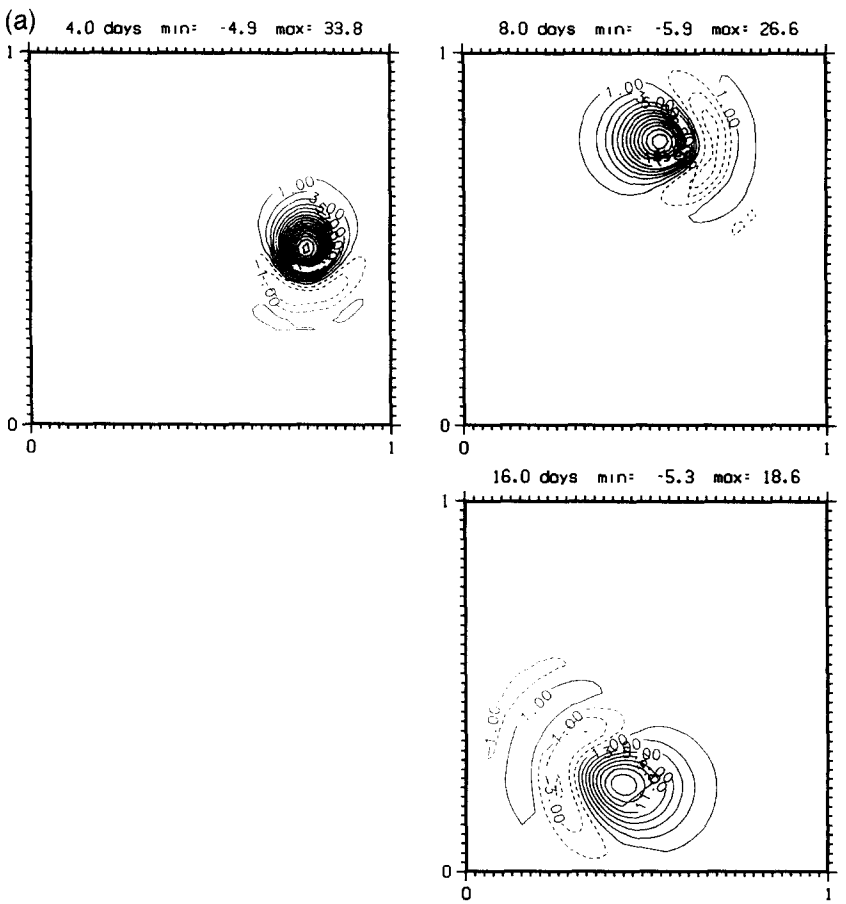

Fig. 1. Passive scalar advection test. The 'order' of the scheme refers only to the interpolations of the advected quantities from the cell centers to the cell faces, where they are multiplied by the specified constant angular velocity field (rigid body rotation) to get the control volume fluxes. Results are shown at time = 4, 8, 12, and 16 days. One full revolution around the mid-point for the specified constant angular velocity advection field occurs in 16 days.

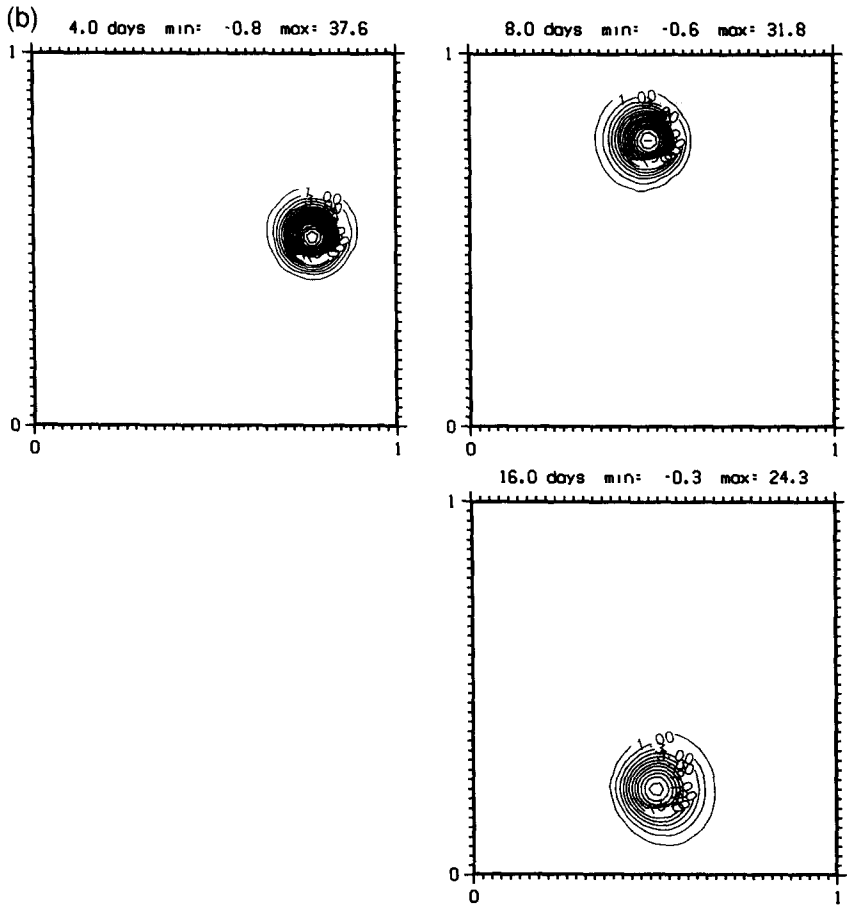

Fig. 1 (continued).

Our passive scalar is assumed to have a shape of a cone with radius four points. The grid is 40 by 40 points. The initial peak (vertex) is given a value of 50. Rigid body rotation (constant angular velocity) is specified for the flow. The initial location of the

Table 1
Percent cone height undershoot error: cyclic passive scalar advection problem. Most-negative height as percentage of initial height after one revolution of cone feature. Cone radius is four grid intervals. Cell-Reynolds number is based on velocity at center of cone in constant angular velocity advection field

Cell RE[a]	Order of interpolation of cone height	
	2nd order	4th order
45	10.6	0.6
90	15.6	4.0

[a]Reynolds number.

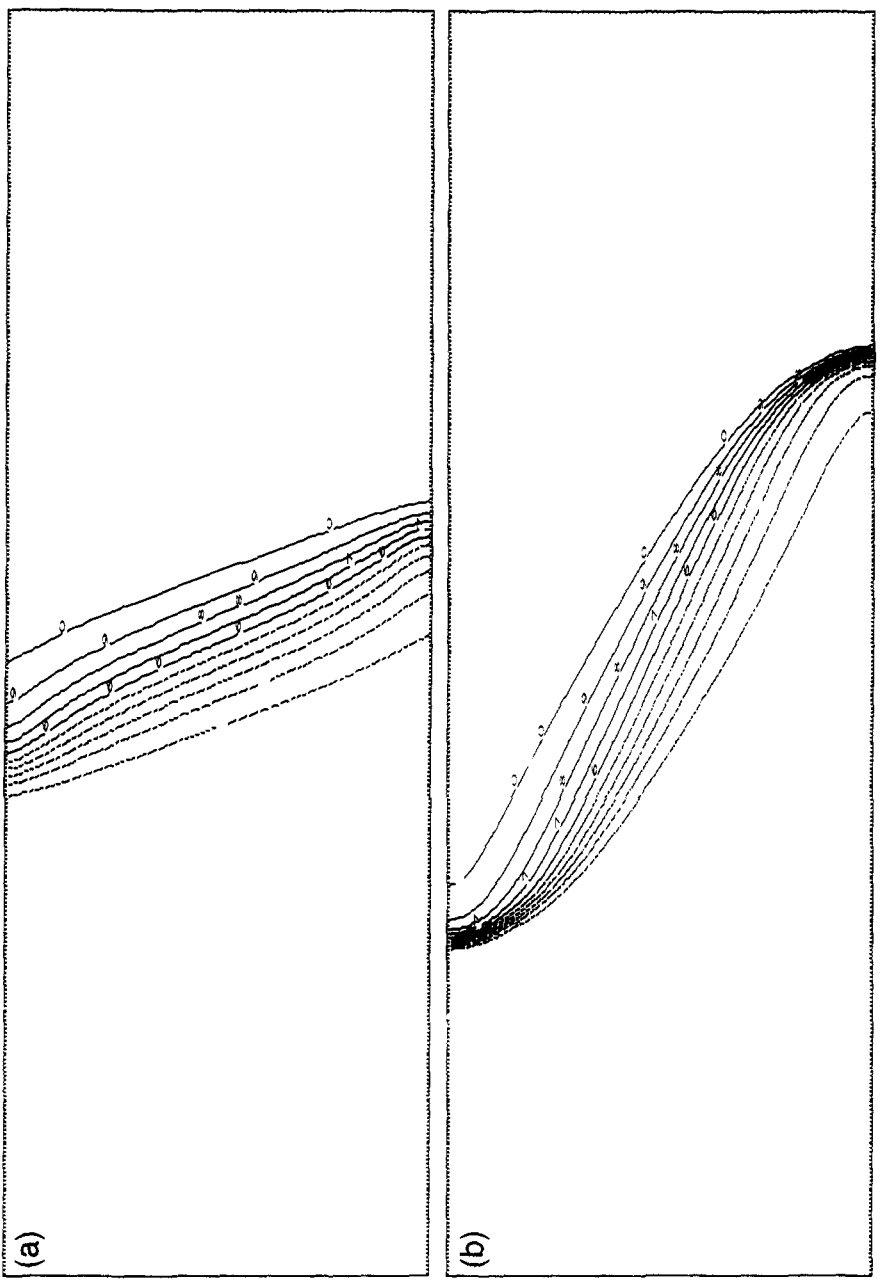

Fig. 2. Sloshing front problem with high (25-m) resolution. Grid size is 400×100. The maximum cell-Reynolds number is about 20. Both RDA and MIA are included. The evolution from an initially vertical front (at time = 0) is shown at times 1, 2, 4, 8, and 12 h. The overshoot errors (beyond the initial extrema of −0.0500 and 0.0500°) at the respective times are: 0.0000, 0.0002, 0.0010, 0.0002, and 0.0003°.

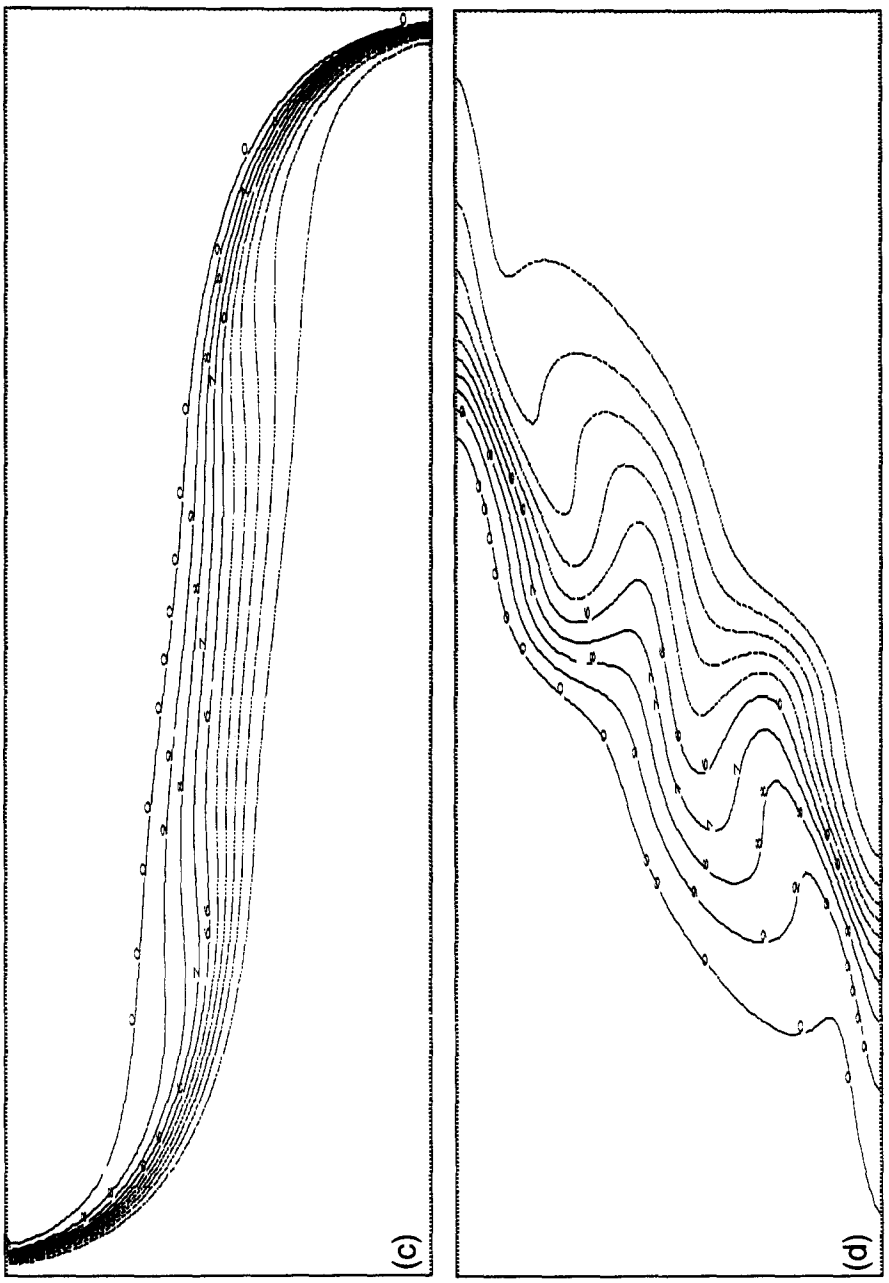

Fig. 2 (continued).

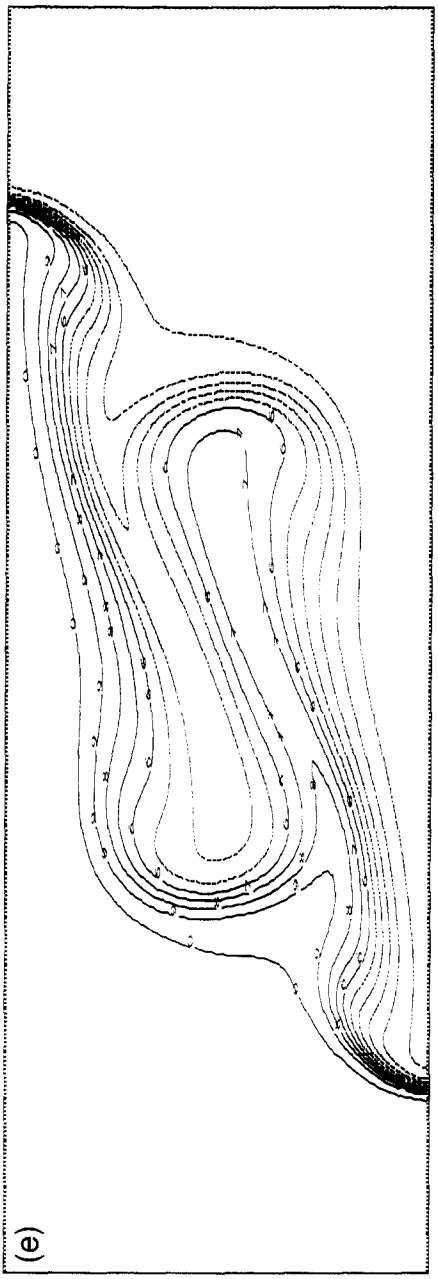

Fig. 2 (continued).

vertex is midway between center of the cylindrical geometry and the sidewall. The time step Courant number is 0.32 at the cone center, 0.8 at the corners of the grid. Runs with high and low passive scalar diffusivities are used, such that the cell-Reynolds number is approximately 45 and 90, respectively, at the cone center. Runs with our modified (four point interpolations) and original (two point interpolations) schemes are performed. The explicit diffusion quickly eliminates the discontinuities at the cone vertex and cone base. Negative values are a result of purely numerical dispersion errors. The results (Fig. 1 and Table 1) demonstrate that RDA is much less dispersive than our original scheme.

3.2. *Non-hydrostatic Boussinesq 2-D sloshing front*

In real applications, numerical models must deal with a dynamically evolving advection velocity. As noted in Section 2, determining such advection velocity on the Arakawa 'a' grid used by the DieCAST model requires interpolations that are numerically dispersive. However, our modified scheme is much less dispersive, as we now show through a second test problem.

Our second test problem involves incompressible non-hydrostatic Boussinesq flow in a two-dimensional closed rectangular cavity. Its scale is 8 km wide by 2 km deep. Model resolutions of 25, 50, and 100 m are used. Rigid free-slip boundaries are assumed. The initial conditions are: zero flow, with a vertical front midway between the sidewalls. Viscosity and thermal diffusivity are 100 $m^2\ s^{-1}$ in all cases. An initial temperature contrast of 0.1°C is specified across the front, and is related to density by a Boussinesq approximation appropriate for water. The resulting flow velocity maximum is about 1 $m\ s^{-1}$, giving a maximum cell-Reynolds number about 20 with the highest resolution.

Fig. 2 shows temperature evolution from its initially vertical front position (not shown) in results using the high resolution (25 m) with both modified schemes, RDA and MIA, described in Section 2. Front positions are shown at times 1, 2, 4, 8 and 12 h after its vertical initial position with cold dense water on the left. The front rotates counterclockwise until the cold fluid and warm fluid are approximately interchanged. Sharp fronts occur along the top and bottom boundaries when the front is substantially away from vertical orientation.

Table 2
Maximum percent temperature overshoot error: sloshing front problem. Non-hydrostatic sloshing front problem with three resolutions. The maximum cell-Reyolds number is about 20 with the highest (25-m) resolution. The 'RDA' scheme improves passive scalar advection; 'MIA' reduces numerical dispersion resulting from interpolations between staggered 'c' grid and collocated 'a' grid used in applying incompressibility condition

Resolution (m)	New schemes included			
	Neither	RDA	MIA	RDA and MIA
25	0	2	0	2
50	31.6	4	34.2	3.8
100	65.6	33.2	97.6	37.8

A measure of the non-linear dispersion error is the maximum temperature above the original, which occurs when the front reaches corners for the first time (about 4 h into the run). The dispersion is not apparent in the plots of Fig. 2. However, at 4 h, the temperature range reaches a maximum value of −0.051 to 0.051 K, which is 2% overshoot beyond the initial range of −0.050 to 0.050, indicating some numerical dispersion.

Table 2 shows these maximum overshoots at all three resolutions for cases with different combinations of RDA and MIA. It shows that RDA has a strong positive effect, while MIA seems to have a weakly negative effect. This negative effect can be explained as follows. Advection overshoots increase as feature size decreases. The reduced dispersion associated with the improved interpolations tightens the front, increasing advection overshoot errors, although the fact that the front is tight can mean more accurate solution in spite of the overshoots.

3.3. Hydrostatic 3-D Gulf of Mexico circulation

Although our Gulf of Mexico model is three-dimensional, the RDA scheme is applied only to horizontal advection. Vertical advection is not involved in the important barotropic (vertically averaged) flow component. However, vertical density advection is a primary term in internal wave propagation. As noted by Dietrich (1993), this suggests that specially accurate treatments of vertical density advection, such as RDA, might be quite useful, especially for baroclinic flow components whose scales are determined by the Rossby radius of deformation and thus by internal wave propagation.

We inserted both MIA and horizontal RDA of Section 2 into our Arakawa 'a' grid Gulf of Mexico model (Dietrich and Ko, 1994) with 20 km resolution. Full details on the physical problem are given by Dietrich and Lin (1994). We ran simulations with the modified and original schemes using identical open boundary and initial conditions, and identical model geometry and parameters. Initial conditions were from Day 1800 of a run with the original schemes.

Within a model time step, the original and MIA schemes both generate an intermediate 'a' grid velocity result, interpolate it to the 'c' grid, and then use pressure adjustment to eliminate the divergence from the 'c' grid velocity. The original scheme then interpolates the non-divergent velocity back to the 'a' grid. In contrast, the MIA scheme interpolates the changes in velocity, made in eliminating its divergence, to the 'a' grid and adds them to the original 'a' grid velocity. Thus, these two schemes give slightly different 'a' grid results. Here, each time step, we combine 3% of the solution resulting from the original scheme with 97% of the MIA result, which gives another slightly different 'a' grid result. This procedure reduces noise although the model is stable with the pure MIA scheme. Increased small-scale noise can lead to increased mixing across

Fig. 3. Gulf of Mexico results with and without RDA and MIA. The two 'identical twin' runs use same initial conditions (at Day 1800), boundary conditions, geometry, and model parameters. The only difference is the numerics. The larger maximum velocities with the new features reflect much tighter fronts, resulting in a well-developed frontal eddy, similar to observations, by Day 1835.

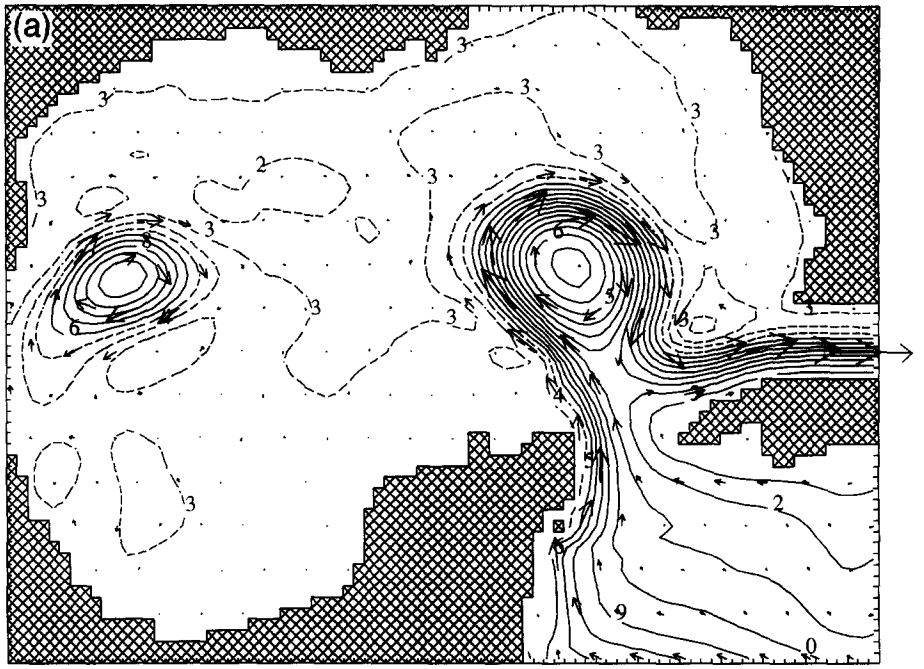

day 1815, Vmax=102.9

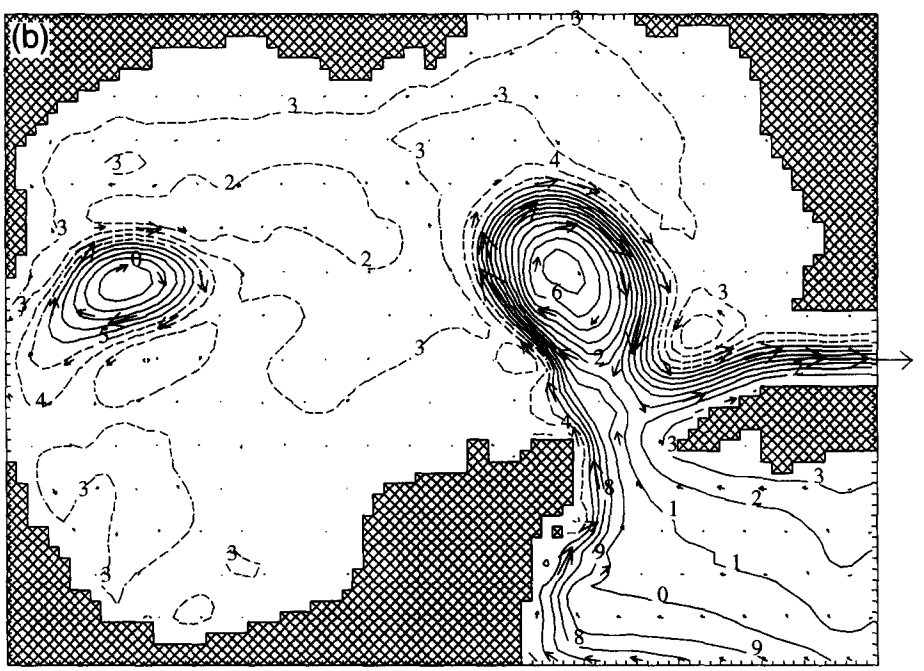

day 1815, Vmax=143.2

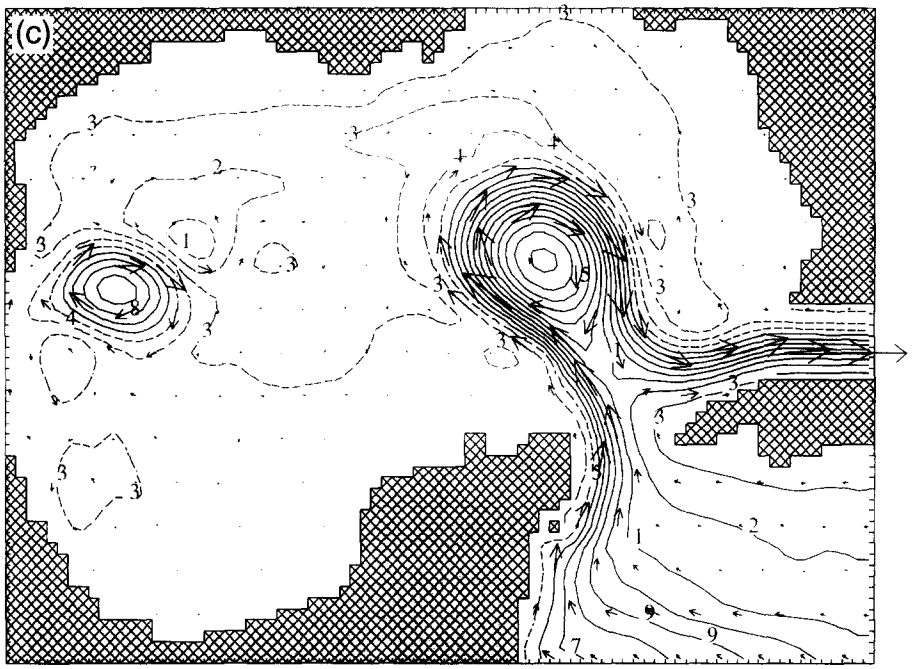

day 1835, Vmax=120.1

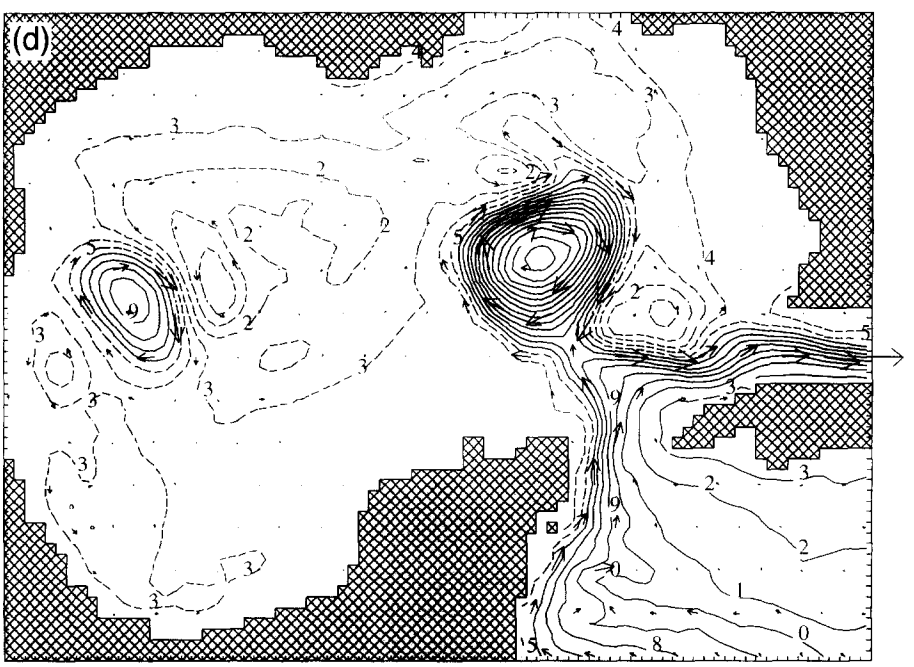

day 1835, Vmax=140.1

Fig. 3 (continued).

fronts, like the effects of eddy viscosity. This increased mixing seems to be unphysically large due to truncation errors in small-scale eddies, because the fronts seem to be diffused and main Loop Current eddies eroded and dissipated more rapidly than typically observed. This excess mixing can be reduced by combining MIA with the more dispersive original scheme.

Figs. 3 and 4, and Table 3, give results with various combinations of the RDA and MIA schemes. Fig. 3(a) and (c) and Fig. 4(a) and (b) show results with the original numerics (neither RDA nor MIA). Fig. 3(b) and (d) show results with both new features. Fig. 3 shows top layer pressure contours (interval = 5 cm equivalent hydrostatic pressure head, which closely matches sea surface height deviation from a level surface) with superposed velocity vectors. A rapid increase of velocity occurs during the first 15 days (Days 1800–1815) with the new features. This increase results from the rapid tightening of fronts caused by reduced numerical dispersion. Starting about Day 15, frontal eddies grow and mix water across the front, thereby limiting the tightening of the fronts. This mixing slows the increase of velocity and makes it more irregular as indicated in Table 3 and Fig. 4. The frontal eddies are much weaker with the RDA scheme by itself (not shown), and the maximum velocity continues to increase at a slower rate (second column, Table 3) through Day 1860.

The dominant frontal eddy on the north side of the larger separating Loop Current eddy in the MIA results (right panel, Day 1835) originated just north of the Yucatan Peninsula (right panel, Day 1815). It is associated with an occluded front pattern much like Fig. 5, which compares surface temperature distribution from satellite observations with those from a higher resolution (9 km) simulation using the original numerics. These kinds of patterns are common in observations and in our model results. The frontal eddy is just a weak frontal wave in the original scheme results (Fig. 3(a) and (c)). Thus, the MIA results appear more realistic and more like the higher resolution results.

In the long run the MIA scheme leads to many more eddies throughout the Gulf of Mexico, and the Loop Current flattens when it sheds an eddy (Fig. 4). Satellite and

Table 3
Effect of new schemes on Gulf of Mexico results maximum velocity (cm s^{-1}) development after initializing with Day 1800 results from run with neither new feature. The original scheme (with neither RDA nor MIA), from which all four runs are initialized at Day 1800, is already in near statistical equilibrium by Day 1800, so we did not run it past Day 2160

Time	New schemes included			
	Neither	RDA	MIA	RDA and MIA
Day 1815	102.9	105.0	135.9	143.2
Day 1830	114.0	117.3	157.2	139.9
Day 1845	116.3	118.2	154.6	145.9
Day 1860	112.1	123.2	131.5	158.3
Day 1920	90.1	–	–	147.5
Day 1980	96.1	–	–	131.3
Day 2160	122.5	–	–	229.8
Day 2520	–	–	–	223.9
Day 2880	–	–	–	161.6

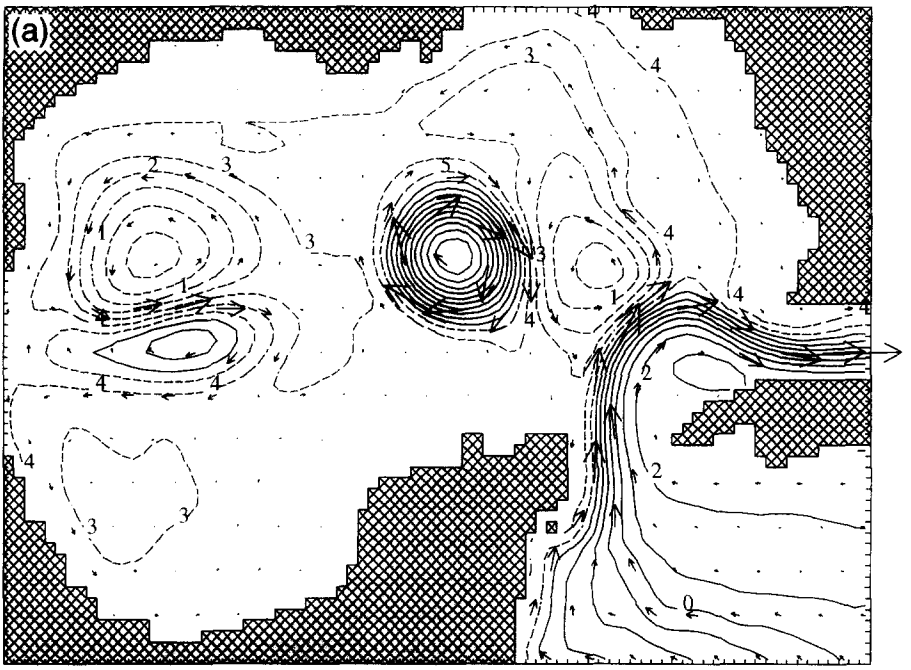

day 2160, Vmax=122.5

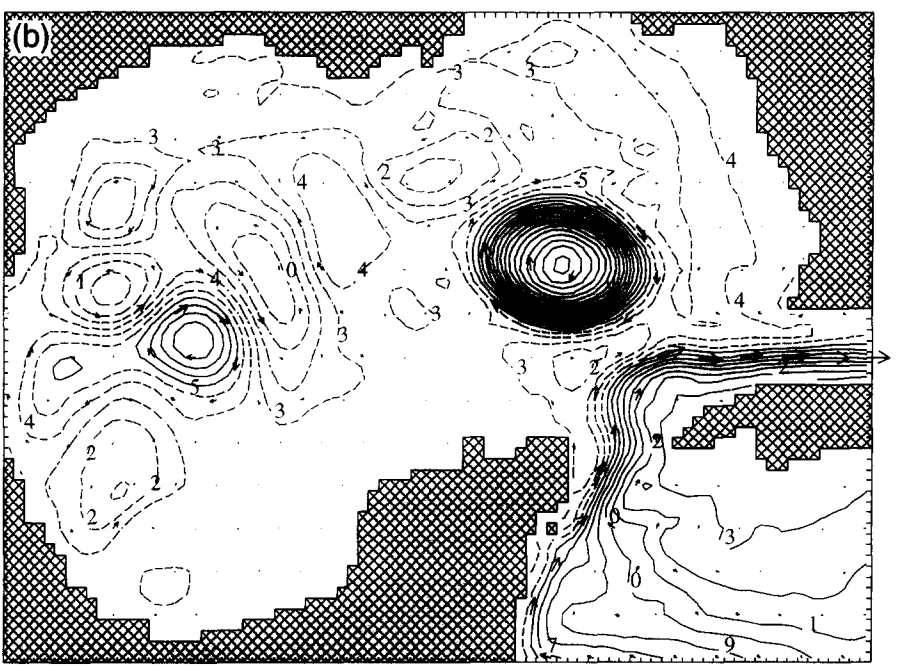

day 2160, Vmax=229.8

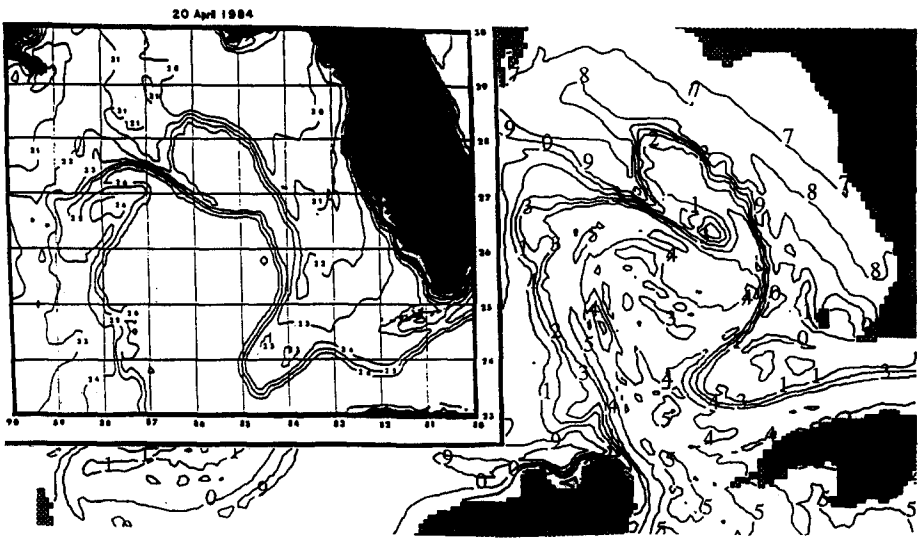

Fig. 5. Top level (depth = 10 m) temperature from the DieCAST model and from observations (inset) in the Gulf of Mexico. The model snapshot is at Day 1220 of a 1/12 by 20 layer numerical simulation. The single-digit contour labels in the model output omit the 10s digit; thus for example the label '5' denotes a temperature of 25°C. The observations are sea-surface temperature derived from a satellite image dated April 20, 1984 (Waddell and Brown, 1987).

drifter observations indicate that there are typically more than a dozen significant eddies in the Gulf of Mexico at a given time (P. Niiler, 1993 personal communication). The Loop Current flattening is also like previous higher resolution simulations and observations. The original scheme is already in near statistical equilibrium at Day 1800, so we do not include results beyond Day 2160 in Table 3.

In Table 3, the RDA scheme has much less effect on the early rapid maximum velocity increase than MIA, in contrast to the results for the non-hydrostatic sloshing front (Section 3.2). This appears related to the rapid growth of the Loop Current frontal eddy between Days 1815 and 1835, which has much reduced amplitude with RDA alone (Fig. 3). Three possible reasons are: RDA was not included in vertical advection; in the absence of MIA, the fronts are less tight and better resolved, so the higher order interpolations of RDA have less effect; and in contrast with the sloshing front problem of Section 3.2, ocean flows tend to be nearly parallel to fronts, so large-scale features develop and propagate by vortex stretching and vorticity advection dynamics associated with Coriolis terms (Rossby waves), rather than by horizontal density advection.

Fig. 4. Gulf of Mexico results at Day 2160. The decreased numerical dispersion with RDA and MIA leads to a more vigorous and widely dispersed eddy field, similar to observations and to higher resolution results (not shown) with the more standard approach (using neither RDA nor MIA).

4. Comments on the modified schemes

The modified schemes decrease numerical dispersion, and lead to tighter fronts and more energetic small-scale frontal eddies. These can mix material across fronts, resulting in 'physical' (involving resolved velocity components rather than interpolations) dispersion. Such physical dispersion can extend the mixing region for different water masses, leading to a more widely distributed eddy field. A good numerical experiment (not done here) might be to add a passive scalar to water within a major Gulf Stream or Loop Current warm core eddy and compare how it disperses with the modified and original schemes. Widely distributed eddy fields may be important, such as in the westward dispersion of Labrador Current cold bottom water along the Grand and Georges Banks, which influences the separation of the Gulf Stream at Cape Hatteras, as we see in recent application of our new numerics to the North Atlantic Basin (Dietrich and Mehra, 1996). For small-scale flow components, such as frontal eddies, such 'physical' dispersion can of course have significant truncation error effects, yet the very existence of the frontal eddies on tight fronts is an improvement in representing nature.

Both modified schemes are robust in application to the propagation of warm core Loop Current eddies across the Gulf of Mexico. This propagation involves highly non-linear dynamics: a strong front is maintained at the outer edge of the warm core eddy as it spins at about one rotation per 15 days while propagating across the Gulf of Mexico over a period of about 6 months. Frontal eddies slowly disperse the warm core water as it spins westward. In the new model results with 20-km resolution, the warm core eddies deform more and lose their identity more rapidly because of this dispersion, but the dispersed energy appears in a much larger number of eddies, as observed. One can reduce this 'physical dispersion rate' by combining our modified reverse interpolation scheme with our original one. Indeed, as results in Section 3.3 indicate, combining only 3% of our original scheme with 97% of the new scheme leads to more realistic overall behavior than the original scheme with 20-km resolution, especially for small-scale flow components.

Although RDA is first-moment conservative, the conservation properties of RDA and MIA are not the focus here. We have seen no indication of non-linear instability, as occurs with some non-quadratic-conserving schemes. Accuracy (which, among other things, means low numerical dispersion) is our primary concern.

5. Concluding remarks

We have discussed two modifications of the schemes used by our original ocean model and explored their effects on greatly different computational fluid dynamics problems. In contrast with the non-hydrostatic sloshing front problem of Section 3.2, the main improvement in the Gulf of Mexico general circulation problem of Section 3.3 appears to be MIA scheme rather than RDA. This probably relates to the fact that, in ocean general circulations, the velocity tends to be nearly parallel to the iso-surfaces of the advected fields, in contrast to the sloshing front problem. Further, when the internal wave terms are treated explicitly (in time) as usually done, the Courant number is

generally quite small. The result is that advection effects are small even for a rather large number of time steps, during which many dispersive interpolations are used in satisfying incompressibility. However, the northern oceans have characteristics perhaps more like those of the sloshing front problem, so both MIA and RDA are of interest in ocean modeling as well as in other computational fluid dynamic applications. Although the present model produces acceptable general circulation patterns in the Gulf of Mexico and is thus a good test for the new methods, it is not applicable to fast modes such as tides because of its rigid-lid approximation. The new methods are, however, applicable to free surface models as well as general circulation models. Much needs to be done to understand the behavior of these schemes in detail, but our present results show that they have interesting effects and are quite promising.

Acknowledgements

I am greatly indebted to Paul Martin for motivating this work through his initial tests of the new numerics and for providing suggestions and comments. This work was supported by the Office of Naval Research under Research Grant N00014-92-J-4109 with Mississippi State University.

References

Dietrich, D.E., 1992. The Sandia Ocean Modeling System Programmers Guide and Users Manual. SAND92-7386, Sandia National Laboratories, Albuquerque, NM 87185.

Dietrich, D.E., 1993. On modeling low Rossby number flows. Atmosphere–Ocean 31, 57–71.

Dietrich, D.E., Ko, D.-S., 1994. A semi-collocated model based on the SOMS approach. Int. J. Num. Methods Fluids 99, 1103–1113.

Dietrich, D.E., Lin, C.A., 1994. Numerical studies of eddy shedding in the Gulf of Mexico. J. Geophys. Res. 99, 7599–7615.

Dietrich, D.E., Mehra, A., 1996. Modeling with DieCAST in the North Atlantic Basin. In: Proceedings of the 1996 Western Pacific Geophysics Meeting (AGU), 23–27 July 1996, Brisbane.

Dietrich, D.E., Marietta, M.G., Roache, P.J., 1987. An ocean modeling system with turbulent boundary layers and topography: numerical description. Int. J. Num. Methods Fluids 7, 833–855.

Dietrich, D.E., Roache, P.J., Marietta, M.J., 1990. Convergence studies with the Sandia Ocean Modeling System. Int. J. Num. Methods Fluids 11, 127–150.

Dietrich, D.E., Ko, D.-S., Yeske, L.A., 1993. On the application and evaluation of the relocatable DieCAST ocean circulation model in coastal and semi-enclosed seas. Technical Report 93-1, Center for Air Sea Technology, Mississippi State University, Stennis Space Center, MS.

Roache, P.J., 1976. Computational Fluid Dynamics. Hermosa Publishers, Albuquerque, NM, 446 pp.

Roache, P.J., Dietrich, D.E., 1988. Evaluation of the filtered leapfrog-trapezoidal time integration method. Numer. Heat Transfer 14, 149–164.

Waddell, E., Brown, M.L., 1987. Gulf of Mexico Physical Oceanography Program Final Report: Year 4, Technical Report. Vol. II. MMS Publication 87-007, US Department of Interior, Minerals Management Service, Gulf of Mexico OCS Region, New Orleans, LA, p. 87.